Study of Short-term Evaporation in Sand Specimens via Micro-focus X-ray Computed Tomography

K Liu; *University of Southampton, MSc, PhD researcher, UK, kl5g14@soton.ac.uk*
F. A. Loveridge; *Royal Academy of Engineering Research Fellow, University of Leeds (formerly University of Southampton), BA MSc PhD, CEng, MICE, FGS, CGeol, UK*
R. Boardman; *μ-vis Centre, University of Southampton, PhD, MInstP, MIEEE, Principal Scientist, UK*
W. Powrie; *University of Southampton, FREng MA PhD, CEng, FICE, Dean Faculty of Engineering and the Environment & Professor of Geotechnical Engineering, UK*

ABSTRACT: Water flow and heat transfer often occur simultaneously in soils, in coupled flow, for example in applications such as ground heat thermal storage and disposal of nuclear waste. It is proposed that micro-focus X-ray computed tomography (micro-XCT) can be used to investigate this phenomenon. A natural thermally-driven water flow, evaporation from an exposed soil specimen, is studied to assess the applicability of micro-XCT techniques to other problems in soil heat / moisture transfer. This paper presents studies of short-term evaporation from a sand. A series of scans were conducted on a specimen of sand during evaporation, to provide data for comparison with simultaneous gravimetric measurements made using a sensitive balance in the scanner. Both qualitative and quantitative data from the micro-XCT are presented. Drying of the specimen during each stage can be clearly seen in the image data. However, quantification of the change in water content by image analysis is more challenging, owing to the compromise between the image quality and the scanning time. To overcome this, an alternative approach to segmentation of the image data using Gaussian curve fitting is proposed and validated against global gravimetric measurements. It is concluded that this approach to the analysis of the rapid movement of moisture within the soil is promising, and it will be applied in future experiments.
KEYWORDS: heat transfer; evaporation; micro-XCT; laboratory testing

1. INTRODUCTION

The coupled phenomenon of water flow and heat transfer is relevant to geotechnical applications such as nuclear waste disposal and ground heat thermal storage. Investigation of these problems requires careful coupled modelling, but practical data for model validation is challenging to obtain. Micro-focus X-ray computed tomography (micro-XCT) offers the potential to investigate these phenomena, both qualitatively and quantitatively.

As a natural thermally-driven water flow, evaporation in soil specimens has previously been studied using XCT techniques by researchers such as Shokri et al. (2009) and (Yang et al., 2015). However, their interests were mainly in long-term evaporation behaviour in soils, where evaporation takes place over a period of days; or the focus was not the temporal evolution of moisture content within the specimen. Synchrotrons can achieve fast scans suitable for assessing rapid changes in soil moisture, and have been used in studies such as Shokri et al. (2010), Shokri and Sahimi (2012) and Wildenschild et al. (2005). However, the field of view is often limited with a synchrotron; and there is generally a lack of comparative gravimetric moisture content measurements.

This paper reports results from a study of short-term evaporation from a sand specimen using micro-XCT techniques. The work develops and validates a method of data analysis that will be applied in future experiments on coupled heat and moisture flow.

2. PRINCIPLES OF MICRO-XCT

In XCT imaging, electrons are generated by a metal filament (cathode), then transported to the X-ray target (anode). X-rays are then produced by the interaction of electrons in the X-ray target, before continuing to image the object. The object is imaged from various orientations as it rotates during the scan (Kak and Slaney, 2001). 2D projection image data are acquired by the detector located behind the object after the entire scanning process is completed. The raw 2D projection data are then reconstructed as 3D volume data in the form of a series of 2D image slices. The XCT acquisition and reconstruction processes are shown schematically Figure 1.

The image can be quantified using units of grey scale (GV), which is closely related to the density of specimen materials. Full quantitative analysis can be carried out, provided the GVs have been calibrated (e.g. via Hounsfield units).

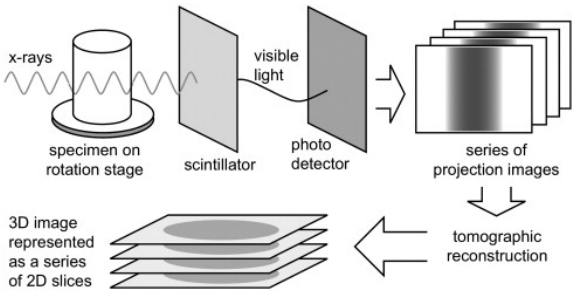

Figure 1. Schematic illustration of XCT acquisition and reconstruction process (Landis and Keane, 2010)

3. EXPERIMENTAL APPROACH

3 .1 *Specimen preparation*

A saturated sand specimen with internal diameter of approximately 5 mm and height of 10 mm was used as the object of the experiment. The material was uniformly-graded Leighton Buzzard sand, with a grain size in the range 90 μm – 150 μm and a grain specific gravity of 2.65. The specimen was prepared by wet pluviation (Raghunandan et al., 2012), immediately before the scanning experiments commenced. In this way, minimal moisture loss occurred before image acquisition started. The detailed dimensions and porosity determined from gravimetric measurement are given in Table 1. The specimen was contained within a polyethylene tube of wall and base thickness 1 mm.

Table 1. Properties of sand specimen

Specimen parameter	Height	Internal diameter	Porosity
	10.05 mm	4.72 mm	44.21%

3 .2 *Experimental setup for CT scans*

The micro-XCT scanner used for the experiments was a Nikon/Metris custom Hutch, featuring the standard 225kVp reflection tungsten target (University of Southampton, 2017). A series of CT scans was conducted using this machine as moisture was lost by evaporation from an initially-saturated sand specimen.

The experimental setup for the CT scans is shown in Figure 3. A balance was placed on the platform of the Hutch scanner to measure the specimen mass during the scanning process. A specially-designed, purpose-built specimen holder was mounted on the balance pan to ensure a repeatable central position of the object. The specimen holder also enabled the X-ray target gun to move close to the specimen to achieve high resolution scans. Finally, the sand specimen was placed on the top of the specimen holder.

A hygrothermograph was placed near the specimen on the same manipulator platform, to measure temperature (T) and relative humidity (RH) during the scanning process. This showed that the environmental conditions inside the scanner cabin were relatively stable, with a temperature (T) of around 19.5°C and the relative humidity (RH) 50%.

Evaporation from a sand specimens of this size is rapid. Trial experiments on three similar specimens (Figure 2) showed that the evaporation would be expected to be largely complete within eight hours. Consequently, rates of change of volumetric moisture content would be expected to be rapid, especially at the start of the test.

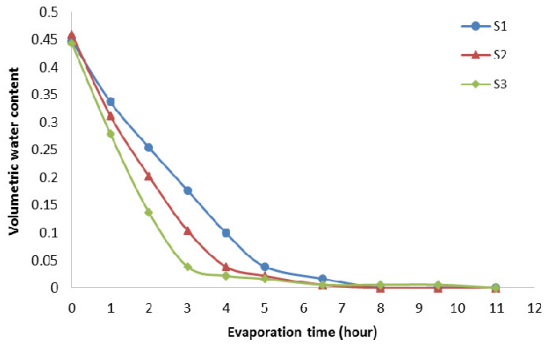

Figure 2. Trial evaporation experiments on this size of specimens

Accordingly, rapid scan times are required to obtain representative data throughout the evaporation period and for comparison with gravimetric measurement. If scan times are too long then there would be blurring of the resultant images due to the moisture drying and movement. However, reducing scan times too much will lead to adverse effects on the image quality. Also, the stability of the specimen or specimen holder could be affected under rapid scan conditions, potentially inducing the movement of the specimen.

Using the scan settings in Table 2, a scan duration of only 7 minutes was achieved. This meant that during a total experiment time of about 8 hours, a 7 minute sampling frequency achieved 64 data points.

Table 2. Scan settings on Hutch

Energy	Intensity	Exposure time	Frames per projection	Projection count	Resolution
70 kV	98 µA	354 ms	1	1201	6.4 µm

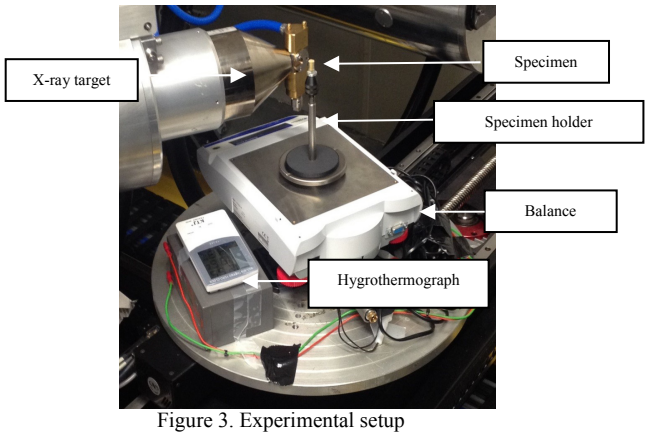

Figure 3. Experimental setup

4. DATA SELECTION AND SEGMENTATION

4 .1 *Region of interest*

A representative region of interest (ROI) was taken from the entire image data for subsequent segmentation and analysis. Owing to the limitations of imaging acquisition and image reconstruction (e.g. cone artefact (Zbijewski and Beekman, 2006) and beam hardening), the ROI was chosen from the middle area, consisting of 80% of the whole specimen (Figure 4). Image data at five typical temporal steps are analysed, 1 hour, 2 hour, 3 hour, 4 hour and 5 hour after evaporation started. The data were then processed and used to explore the suitability of the image analysis techniques. To complete the analyses, it was first necessary to develop segmentation methods using the 0 hour and 8 hour data sets as a benchmark. This is described below.

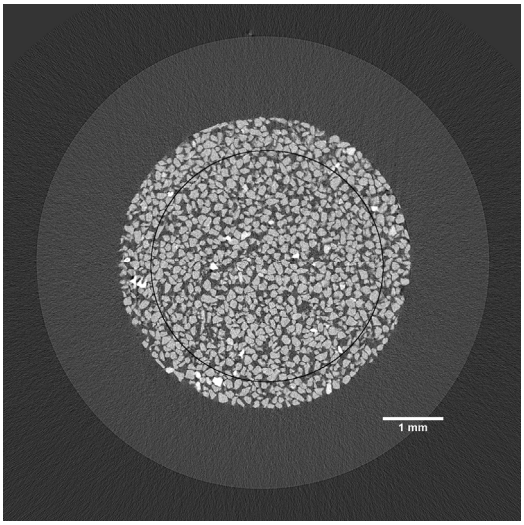

Figure 4. ROI for sand specimen

4 .2 *Segmentation*

Segmentation is the process of splitting up the images obtained from the CT scan into sets of pixels. In this case, the sets of pixels represent the solid, pore fluid and pore air phases of the soil specimen. The simplest method of segmentation is thresholding. The thresholds are used to separate ranges of grey value (GV) and hence distinguish between the different phases. However, established methods of thresholding, such as the commonly used Otsu method (Otsu, 1975), are not effective when the contrast between the GVs of two phases is poor. This is the case for air and water

in unsaturated soil specimens, and the problem is exacerbated in the current application by the fast scan times. Consequently, an alternative approach based on Gaussian curve fitting is explored in this paper.

4 .3 *Gaussian curve fitting*

The GV statistics of image data can be sensibly assumed as Gaussian distributions, which appear as the density function of normal distributions. Previous work, such as Anniballe and Bonafoni (2015) and Anthony and Granick (2009), has adopted Gaussian curve fitting for image analysis, although not for use with geotechnical image data.

In this case, Gaussian curve fitting is implemented using the Levenberg-Marquardt algorithm (Levenberg, 1944; Marquardt, 1963). For convenience, the fitting is carried out using the mathematical plotting package Gnuplot (Williams *et al.*, 1986).

The typical formula for a Gaussian distribution can be represented by Eq. (1), where σ is standard deviation, μ is mode GV and a is the area under the Gaussian curve. The three coefficients are the unknown variables to be fitted based on the corresponding raw data. Each phase is written as an individual Gaussian equation, with the sum of all then fitted to the raw GV data from the images.

$$f(x) = \frac{a}{\sqrt{2\pi}\sigma} e^{\frac{-(x-\mu)^2}{2\sigma^2}} \qquad (1)$$

Importantly, σ will be the same for all phases in the same scan data since the imaging conditions are the same. However, σ will be different in each temporal scan as the partial volume effects will change with the relative proportions of the phases.

The initial input values of the three unknown variables for two-phase conditions (saturated and dry scans at 0 hours and 8 hours respectively) can be obtained from the statistics of the raw data, on which the fitting process is firstly implemented. The fitting plots based on the determined coefficients are shown in Figure 5 for the saturated condition and Figure 6 for dry condition. In both figures, the thick curve represents the raw data and the thin curve the fitted one. The area underneath the curve represents the corresponding phase proportion, with the low density phase (air/water) at the left and the high density phase (solid) at the right. It can been seen that the magnitude of the trough between the phases is never perfectly fitted. However, later analysis shows that the fit is acceptable in terms of producing data on the phase proportions to sufficient degree of accuracy.

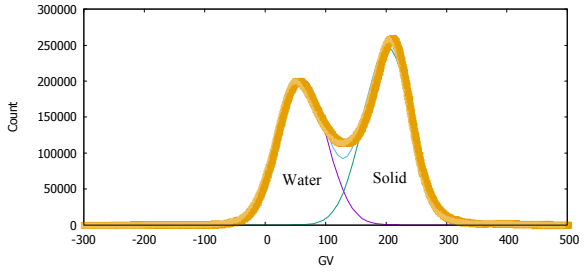

Figure 5. Fitting plot for saturated conditions (0 hours). Green = solid phase; purple = water phase; blue = sum of Gaussians

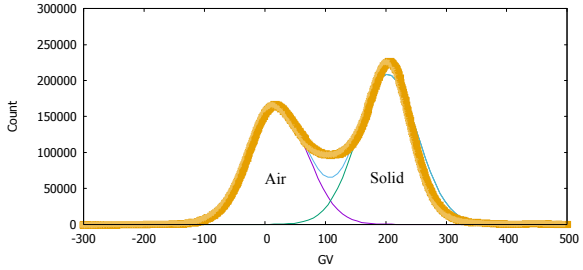

Figure 6. Fitting plot for dry conditions (8 hours). Green = solid phase; purple = air phase; blue = sum of Gaussians

To fit Gaussian curves to the unsaturated data (hours 1 to 5), the coefficient of mode GV (μ) for all the three phases along with the coefficient of area (a_3) for the solid phase are fixed as constant. This assumption is reasonable because the scan settings are the same for all the images and the portion of the solid phase is stable in the sand specimen.

Based on the results for the saturated and dry specimens (figures 5 and 6) the values for the fixed coefficients for fitting in unsaturated conditions are given in Table 3.

Table 3. Determined coefficients for fitting of unsaturated conditions

Coefficient	Determined value
μ1 [Air]	20
μ2 [Water]	61
μ3 [Solid]	203
a3 [Solid]	2.47e+007

5. RESULTS AND DISCUSSIONS

5 .1 *Qualatitive Results*

5.1.1 *GV distribution*

The progression of the pore air phase during evaporation can be seen from the change of GV, as GV is closely correlated with specimen density. As the moisture content reduces during evaporation, the GV decreases accordingly. As can be observed from Figure 7, the GVs from the hourly scanned data during evaporation shows a consistent decreasing relationship, with the highest GV data for the evaporation after 1 hour and the lowest GV value for the evaporation after 5 hours. The magnitude of the GV difference between the different scans is consistent with an evaporating soil specimen, as evaporation happens quickly in the early stage and gradually becomes slower.

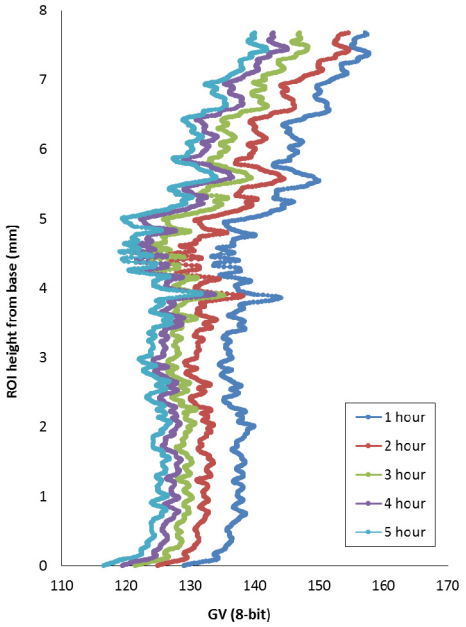

Figure 7. GV distribution through the ROI height of sand specimen

The GV distribution shows that the specimen is relatively uniform through the lower 5 mm region. However, the upper 3 mm seems to be denser, probably as a result of the method of specimen preparation. The very small size makes it difficult to prepare a completely uniform specimen. Also, a small disturbance could affect the density; it is possible that the denser upper section is associated with levelling the top surface of the specimen to obtain a flat finish. Also, when the sand is poured it can form a cone in the upper region of the specimen, preventing the following sand grains from falling uniformly through the de-aired water layer during pluviation.

5.1.2 *Visualisation from temporal images*

As well as observing the evaporation process from the GV distribution, drying can be seen in the CT images directly. As can be observed from Figure 8, the pore space gradually becomes darker as evaporation progresses. This means the air phase (which is the dark region in the CT images) becomes more and more significant. It is also possible to observe the denser layer at the top part of the specimen, where the lighter-coloured sand grains are more tightly packed.

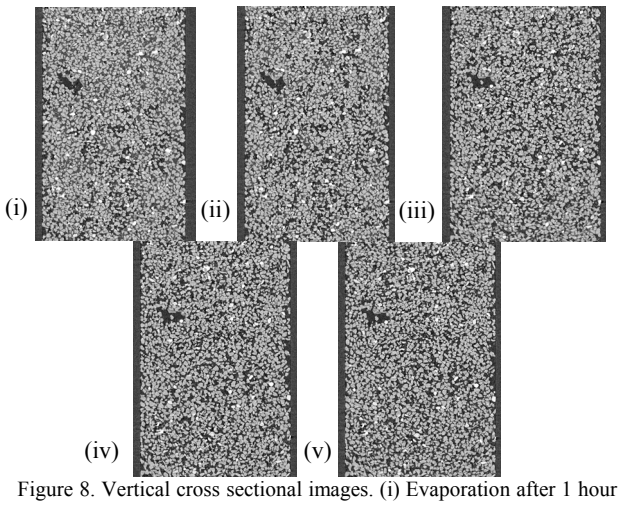

Figure 8. Vertical cross sectional images. (i) Evaporation after 1 hour (ii) Evaporation after 2 hour (iii) Evaporation after 3 hour (iv) Evaporation after 4 hour (v) Evaporation after 5 hour.

5 .2 *Quantative Results*

5.2.1 *Comparison of porosity*

Porosity within the sand specimen was determined from both gravimetric measurements and from analysis of the CT data (Table 4). For the CT, data the volumetric phase proportions were obtained directly from the Gaussian parameter “a”. The similarity of the results shows the reliability of the fitting approach using the two-phase data. This then provides suitable input values for the fitting analysis of the unsaturated cases.

Table 4. Comparison of porosity

	Gravimetric measurement	Saturated condition	Dry condition
Porosity	44.21%	45.23%	44.37%

5.2.2 *Fitting plots for unsaturated cases*

Analysis in unsaturated conditions was initially carried out by Gaussian curve fitting. The five graphs shown in Figure 9 present the fitting results for the five hourly scan data, along with the corresponding raw data for comparison.

Based on the fixed solid curve (at the right hand side), the evolution of the air phase (left hand curve) and the water phase (middle curve) can be clearly observed; the area underneath the fitted curve for the water phase gradually reduces as that for the air phase increases.

The fitting errors for the coefficients *a1 and a2*, which are related to the areas of air and water, are compared in Table 5. It can be seen that the fits for unsaturated conditions are not as close as for two-phase conditions. This is because there are more coefficients in three-phase unsaturated conditions than in the two-phase case.

Table 5. Error of unsaturated fitting results

Fitting error	1 hour	2 hour	3 hour	4 hour	5 hour	Two-phase
a1 [Air]	2.58%	0.78%	0.68%	0.60%	0.48%	0.20% [0 hrs]
a2 [water]	0.36%	0.69%	1.01%	3.20%	2.74%	0.17% [8 hrs]

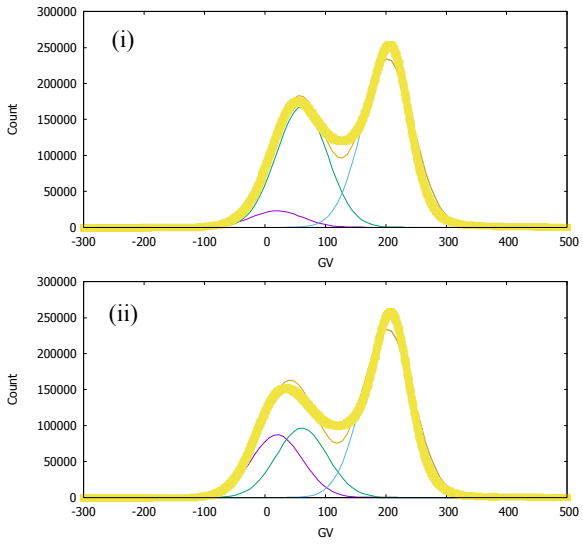

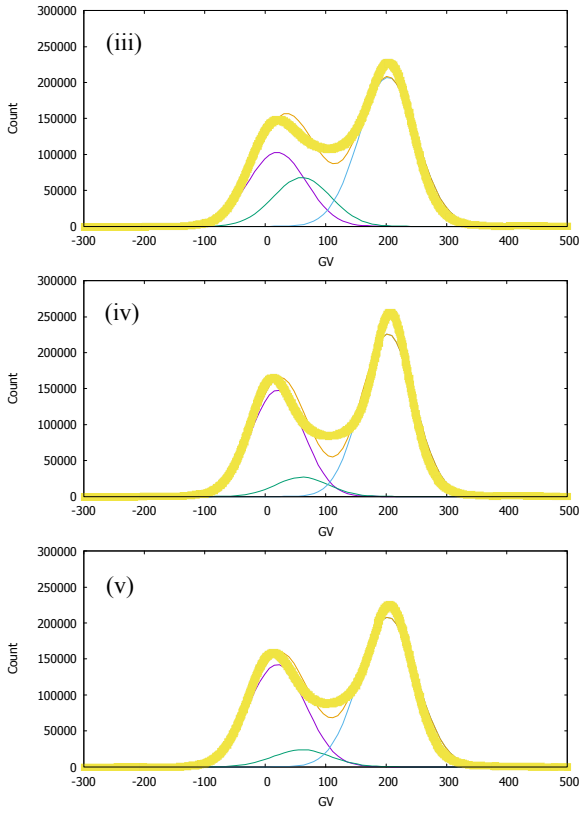

Figure 9. Gaussian fitting for unsaturated condition. (i) Evaporation after 1 hour (ii) Evaporation after 2 hour (iii) Evaporation after 3 hour (iv) Evaporation after 4 hour (v) Evaporation after 5 hour. Yellow = raw data; blue = solid; green = water; purple = air; orange = sum of Gaussians.

5.2.3 *Quantitative analysis of water progression*

Based on the Gaussian fitting for the unsaturated cases, the area of each phase and then the proportion within the specimen is determined for each evaporative temporal step. The results for the air proportion (or cumulative loss of volumetric moisture) are given in Table 6. It can be seen that the phase proportions obtained from the middle three hours for both gravimetric and CT assessment are fairly consistent. However, there are discrepancies between the results in the first and fifth hours.

Table 6. Comparison of air progression

Air %	1 hour	2 hour	3 hour	4 hour	5 hour
Gravimetric measurement	10.44%	19.62%	28.15%	36.68%	43.42%
CT analysis	5.42%	20.90%	27.28%	36.82%	38.03%

For the first hour result, the loss of moisture measured by the gravimetric method is 5% greater than that from the CT data. This could be because initially, water on the top layer of the specimen dries first. However, the ROIs from the CT, chosen to minimise the effect of image artefacts, do not necessarily cover all of this region. Also, small air volumes developed in the first hour of the evaporation, for example in the smallest pores, may not be accurately captured by the analysis of the CT data. This is because of the partial volume effect at the interfaces between different phases, especially when the size of small air regions is comparable with the spatial resolution.

Similarly, there is about a 5% discrepancy between the results of the fifth hour evaporation data. This could be because, when a significant percentage of the moisture content exists as gas (i.e. water vapour) in the later stages of evaporation, its corresponding GV could be similar to that for the water phase, and hence potentially captured by the curve fitting analysis in error. However, the water vapour does not feature in the gravimetric measurement, causing a difference in the results. Furthermore, residual moisture exists in the sand specimen in the form of the meniscus, even when the specimen has effectively ceased drying. If this fraction is significant, together with the partial volume effect at interfaces, it would contribute to the error. Finally, there was some movement of the specimen stage towards the end of the experiment, which could have affected the Gaussian fitting of the final scans.

The degrees of saturation calculated using both methods are shown in Table 7 and Figure 10. Again, the results from middle of the evaporation period are close, with differences less than 5%. The first and the fifth hour show differences of 12%.

Table 7. Comparison of saturation

Saturation	1 hour	2 hour	3 hour	4 hour	5 hour
Gravimetric measurement	0.76	0.56	0.36	0.17	0.02
CT analysis	0.88	0.53	0.40	0.15	0.14

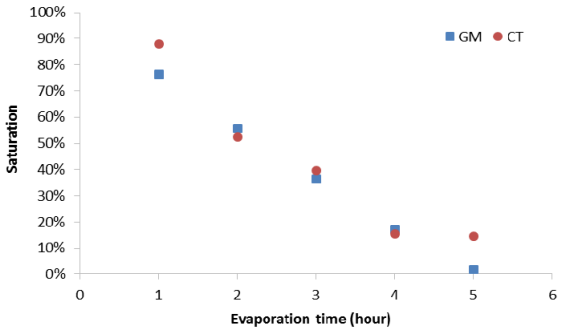

Figure 10. Progression of saturation during evaporation

In summary, the image analysis approach is useful for detecting detailed moisture movement in soils, particularly over the middle ranges of saturation during drying by evaporation.

6. CONCLUSION

The problem of water flow in soils is important in geotechnics, however, it is often difficult to obtain detailed, high quality experimental data. Micro-XCT offers a potential approach, although it is challenging to apply to rapid drying because of the necessary compromise between high quality image data and a short scan time.

In this paper, Gaussian curve fitting techniques were adopted for micro-XCT data of short-term evaporation from a sand specimen. This technique was used to distinguish phases with similar densities (i.e. unsaturated soil phases in this case), and was validated by global gravimetric measurement. However, errors occur when one of the two phases with similar densities (air and water) is present in only small volumes (i.e., in the near-saturated and near-dry conditions). Generally, the Gaussian curve fitting method offers an appropriate way to interpret image data when the quality is reduced (e.g. data obtained from fast scans), although its applicability may be restricted under certain conditions (i.e. a high or a low degree of saturation).

The method described in this paper offers a promising approach for the study of fast moisture movement scenarios in geotechnics using micro-XCT techniques.

7. ACKNOWLEDGEMENTS

The authors would like to acknowledge the Royal Academy of Engineering, the Doctoral Training Centre (CDT) at University of Southampton and EPSRC (grant number EP/G036896/1), who collectively funded this project. All data supporting this study are openly available from the University of Southampton repository.

8. REFERENCES

Anniballe, R. and Bonafoni, S. (2015) A Stable Gaussian Fitting Procedure for the Parameterization of Remote Sensed Thermal Images. Algorithms, 8 (2), 82-91.

Anthony, S.M. and Granick, S. (2009) Image analysis with rapid and accurate two-dimensional Gaussian fitting. Langmuir, 25 (14), 8152-8160.

Kak, A.C. and Slaney, M. (2001) Principles of computerized tomographic imaging. Society for Industrial and Applied Mathematics.

Landis, E.N. and Keane, D.T. (2010) X-ray microtomography. Materials Characterization, 61 (12), 1305-1316.

Levenberg, K. (1944) A method for the solution of certain non-linear problems in least squares. Quarterly of applied mathematics, 2 (2), 164-168.

Marquardt, D.W. (1963) An algorithm for least-squares estimation of nonlinear parameters. Journal of the society for Industrial and Applied Mathematics, 11 (2), 431-441.

Otsu, N. (1975) A threshold selection method from gray-level histograms. Automatica, 11 (285-296), 23-27.

Raghunandan, M., Juneja, A. and Hsiung, B. (2012) Preparation of reconstituted sand specimens in the laboratory. International Journal of Geotechnical Engineering, 6 (1), 125-131.

Shokri, N., Lehmann, P. and Or, D. (2009) Critical evaluation of enhancement factors for vapor transport through unsaturated porous media. Water resources research, 45 (10).

Shokri, N., Lehmann, P. and Or, D. (2010) Liquid-phase continuity and solute concentration dynamics during evaporation from porous media: Pore-scale processes near vaporization surface. Physical Review E, 81 (4), 046308.

Shokri, N. and Sahimi, M. (2012) Structure of drying fronts in three-dimensional porous media. Physical Review E, 85 (6), 066312.

University of Southampton (2017) μ-VIS: Multidisciplinary, Multiscale, Microtomographic Volume Imaging. Available from: http://www.southampton.ac.uk/muvis/about/index.page [Accessed 26th March].

Wildenschild, D., Hopmans, J., Rivers, M. and Kent, A. (2005) Quantitative analysis of flow processes in a sand using synchrotron-based X-ray microtomography. Vadose Zone Journal, 4 (1), 112-126.

Williams, T., Kelley, C., Bröker, H.-B., Campbell, J., Cunningham, R., Denholm, D., Elber, G., Fearick, R., Grammes, C. and Hart, L. (1986) An Interactive Plotting Program. Environment, 4 (10Exit), 5.

Yang, F., Griffa, M., Bonnin, A., Mokso, R., Bella, C., Münch, B., Kaufmann, R. and Lura, P. (2015) Visualization of water drying in porous materials by X-ray phase contrast imaging. Journal of microscopy, 261 (1), 88-104.

Zbijewski, W. and Beekman, F.J. (2006) Efficient Monte Carlo based scatter artifact reduction in cone-beam micro-CT. Medical Imaging, IEEE Transactions on, 25 (7), 817-827.